THE JOURNAL OF
PHYSICAL
CHEMISTRY B
LETTERS

2005, *109,* 6925−6928
Published on Web 03/24/2005

Laser-Induced Gold Deposition on p$^+$-Si from Liquid Precursors: A Study on the Reduction of Gold Ions through Competing Dember and Seebeck Effects

Géza Tóth, Krisztián Kordás, Jouko Vähäkangas, and Antti Uusimäki

*Microelectronics and Materials Physics Laboratories, University of Oulu, P.O. Box 4500,
FIN-90570, Oulu, Finland*

Thomas F. George*

*Office of the Chancellor and Center for Molecular Electronics, Departments of Chemistry & Biochemistry and
Physics & Astronomy, University of Missouri-St. Louis, St. Louis, Missouri 63121*

László Nánai

Department of Physics, JGYTF, University of Szeged, H-6720 Szeged, Boldogasszony sgt. 6, Hungary

Received: January 12, 2005; In Final Form: March 11, 2005

Gold micropatterns are deposited from aqueous solutions of $NaAuCl_4$ on boron-doped Si(100) surfaces ($\rho = 1.5 \times 10^{-4}\ \Omega$ m) using a focused Ar$^+$ laser beam (TEM$_{00}$, $\lambda = 488$ nm, $w_0 = 1.5\ \mu$m, $P = 20-80$ mW). The finite-element method employed for computing the surface temperature profiles reveals that the maximum temperature at the precursor/silicon interface increases only to the range 316−372 K, which is not high enough for chemical reactions with formaldehyde in the precursor. This suggests a different mechanism to be responsible for the reduction of gold ions, namely, changes in the surface potential of Si caused by the Dember and Seebeck effects.

Introduction

The deposition of a number of different metals on semiconductor surfaces from liquid electrolytes using localized light sources has been reported in the literature for over 20 years.[1−9] In most cases, the deposition is explained with photoinduced electrochemical reactions progressing at the solution−semiconductor interface because of the formed Dember potential U_{Dember} and thermal electromotive force U_{Seebeck}.

The goal of this work is to compute the spatial $T(r)$ and temporal $T(t)$ evolution of the surface temperature by solving the heat-flow equation with a commercial finite-element software for the deposition process and to reveal both the temperature-dependent Dember and Seebeck potentials, which all are thought to be responsible for the localized chemical reactions in similar systems. The role of formaldehyde as an additional reducing chemical in the precursor is also discussed, and a novel mechanism for the laser-assisted deposition of gold from aqueous precursors on p$^+$-Si is proposed.

Experimental Setup

The experimental setup consists of a focused Ar$^+$ laser (continuous wave TEM$_{00}$, $\lambda = 488$ nm, $w_0 = 1.5\ \mu$m @ 1/*e* intensity, $P = 20-80$ mW, $I_0 = 2.86 \times 10^9 - 11.44 \times 10^9$ W m^{-2}) and an *xyz* translation stage. The deposition was carried out on p$^+$-boron-doped ($\rho = 1.5 \times 10^{-4}\ \Omega$ m) Si(100) wafers immersed in aqueous electrolytes of (p$_1$) 10^{-2} M $NaAuCl_4$ or (p$_2$) 8×10^{-3} M $NaAuCl_4$ and 2.5 M HCOH.

Results and Discussion

It is found that formaldehyde in the precursor has an important role in the metal deposition. Without formaldehyde, only a thin gold film forms on the laser-irradiated area, and then, the localized plating stops. When formaldehyde is added to the Au^{3+} solution, the growth of the deposits is found to be continuous over time. The deposition does not stop even when the optical transmission of the Au film decreases significantly, indicating that a chemical reaction is proceeding, whereas the laser beam is a heat source rather than a photon source. The role of surface quality in the deposition mechanism is critical. On surfaces covered with thermal oxide (∼500 nm), gold growth does not take place. When wafers with a native oxide layer (∼1 nm) are used, gold nanocrystallites are formed and agglomerated on the irradiated area, leading to a dense Au film after a few seconds (Figure 1).

To compute the spatial and temporal evolution of the surface temperature at the laser spot, the three-dimensional heat-flow equation is solved numerically utilizing the finite-element method, where the source term (the nonreflected power density) is applied as a load

$$c\rho \frac{\partial T}{\partial t} - \nabla(\kappa \nabla T) = (1 - R_{\mathrm{air,precursor}})T_{\mathrm{precursor}} \times (1 - R_{\mathrm{precursor,Si}})\alpha_{\mathrm{opt}}\, \mathrm{e}^{-\alpha_{\mathrm{opt}} z}\, I_0 \exp\left(\frac{r^2}{w_0^2}\right) \quad (1)$$

During the course of the calculations, temperature-dependent

10.1021/jp050222p CCC: $30.25

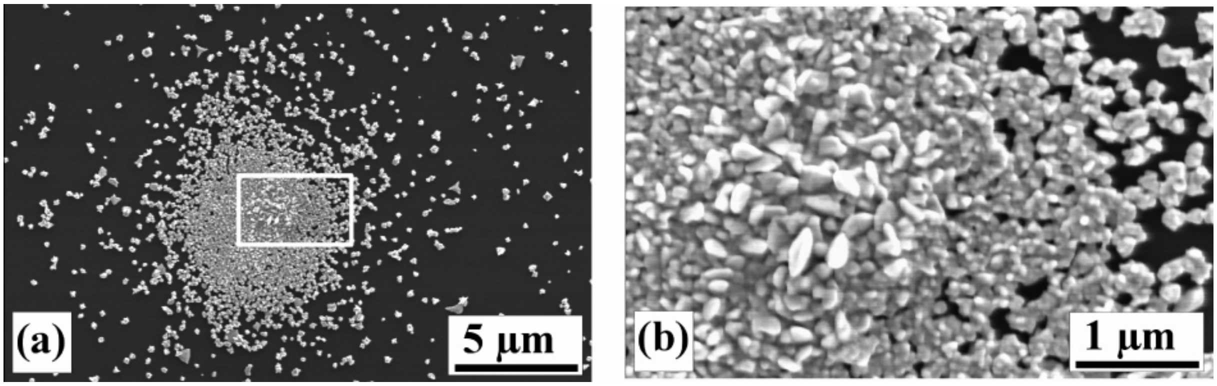

Figure 1. FESEM images of a gold microspots on p^+-Si deposited from an aqueous precursor of 8×10^{-3} M $NaAuCl_4$ and 2.5 M HCOH using a focused Ar^+ laser beam.

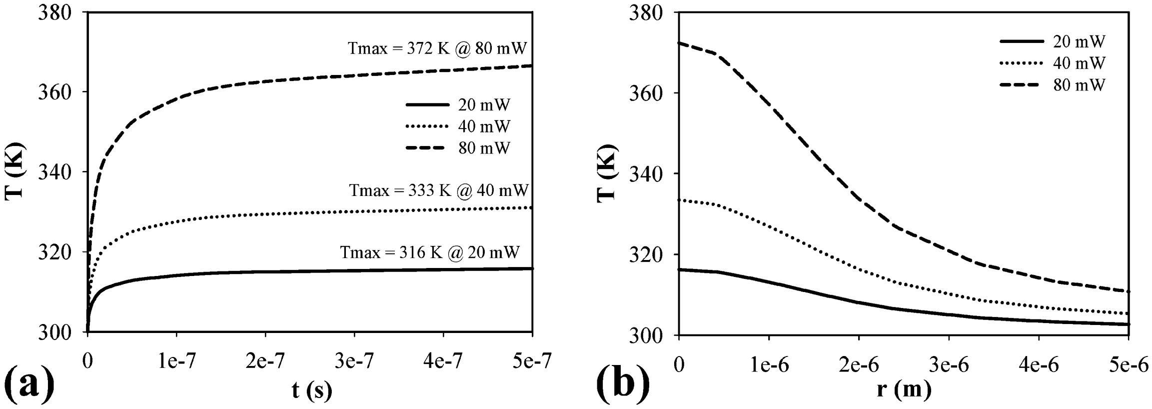

Figure 2. Solutions of the heat-flow equation (eq 1) by the finite-element method under different illumination powers: (a) $T(r = 0, t)$ and (b) $T(r, t = \infty)$.

material parameters of silicon such as specific heat c, density ρ, and thermal conductivity κ are applied. $R_{\mathrm{air,precursor}}$ and $R_{\mathrm{precursor,Si}}$ are the reflectivity of the air−precursor and precursor−silicon wafer interfaces; $T_{\mathrm{precursor}}$ is the transmission of the precursor; α_{opt} is the linear absorption coefficient of the substrate at the laser wavelength under consideration; I_0 and w_0 are the laser parameters (maximum intensity and beam radius); r is the distance from the center of the spot. The change in surface reflectivity, due to the increasing metal coverage during the process, is ignored, because the calculated values of the reflectivity of the precursor−silicon wafer and precursor−gold interfaces for smooth surfaces are very close to each other (0.28 and 0.36, respectively). In addition, the deposited gold surfaces have a roughness of 100−200 nm, decreasing the reflectivity so that the two values are even closer in practice. The applied optical parameters are $R_{\mathrm{air,precursor}} = 0.02$, $T_{\mathrm{precursor}} = 0.98$, $R_{\mathrm{precursor,Si}} = 0.28$, and $\alpha_{\mathrm{opt}} = 1.56 \times 10^{-6}\ \mathrm{m}^{-1}$.

The results of modeling show a rapid but moderate temperature increment of the Si surface for the laser powers applied (Figure 2).

Such low temperatures do not explain the reduction of Au^{3+} ions with HCOH nor the decomposition of $[AuCl_4]^-$ complexes. In addition, a pure thermal process does not explain the effect of the surface oxide thickness on the deposition; hence, the mechanism of gold deposition is governed by other phenomena occurring along the laser−matter interaction. (Note: To verify the reliability of modeling results, a control experiment is carried out, where the laser power is increased until the surface melting point is reached at the focal spot (~640 mW). The calculated peak temperature for such power is very close to the data published in the literature: $T_{\mathrm{m,calculated}} = 1722$ K and $T_{\mathrm{m,literature}} = 1687$ K.)

At the beginning of the process, when there are no deposits or the gold film is transparent, the absorbed photons ($h\nu \approx 2.56$ eV) generate electron−hole pairs, which in turn diffuse from the illuminated zone because of the formed carrier concentration gradients. Because of the higher mobility of electrons compared to the holes ($\mu_n = 2.5 \times 10^{-2}\ \mathrm{m^2\ V^{-1}\ s^{-1}}$ and $\mu_p = 1.5 \times 10^{-2}\ \mathrm{m^2\ V^{-1}\ s^{-1}}$), the illuminated volume becomes positively charged, while negative charge accumulation takes place in the dark field, resulting in a potential difference between the bright and dark zones (Dember effect).[10−12] Besides the mobilities of carriers, the Dember potential is strongly affected by the electron−hole generation rates and carrier lifetimes. For homogeneous illumination (i.e., charge separation in the semiconductor occurring only along the normal vector of the surface), the resulting potential is described as[10−12]

$$U_{\mathrm{Dember}} = \frac{kT}{q}\frac{(b-1)}{(b+1)}\ln\left[1+\frac{(b+1)\Delta n}{n_0+bp_0}\right] \qquad (2)$$

where k is Boltzmann's constant, q is the elementary charge, and $b = \mu_n/\mu_p = 1.67$; n_0 and p_0 are the equilibrium electron and hole concentrations obtained from the temperature-dependent intrinsic carrier density; $n_i(T) = 2[(2\pi kT)/(h^2)]^{3/2}(m_n^*\, m_p^*)^{3/4}\, e^{-E_g/2kT}$ with $n_i^2 = n_0 p_0$, where E_g is the energy gap between the valence and conductive bands; and m_p^* and m_e^* are the effective masses of the holes and electrons. In the case of high impurity levels, the concentration of holes equals the concentration of ionized acceptor impurities, $p = N_a$. On the basis of the results published by Chun,[13] the degree of ionization is well-described by the empirical formula $N_a = 1/\{1 + [(T)/(T^*)]^{-2}\} \times N_{\mathrm{total}}$, where T^* corresponds to the temperature at which one-half of the acceptors are ionized, and $N_{\mathrm{total}} = 1.4 \times 10^{24}\ \mathrm{m}^{-3}$

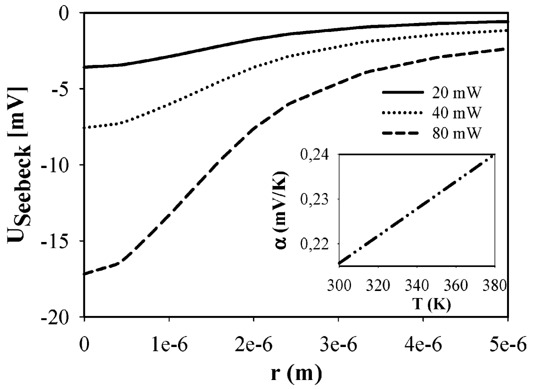

Figure 3. Profiles of the formed thermoelectromotive forces on p$^+$-Si in equilibrium using different laser powers. The inset shows the calculated temperature dependence of the Seebeck coefficient.

is the concentration of acceptor impurities. Assuming that all the photons absorbed create an electron−hole pair, the excess carrier concentration is Δn $(= \Delta p) = P\alpha_{\text{opt}}\tau_{\text{rec}}/h\nu$, where τ_{rec} is the recombination lifetime of free carriers. For large generation rates, τ_{rec} lies in the range from 3×10^{-10} to 10^{-11} s as obtained from photoconductivity measurements by Tzanetakis et al.,[14] so that the calculated excess carrier density is between 1.1×10^{23} and 4.4×10^{23} m^{-3}. This is in good agreement with the observed and calculated relationships between the effective lifetime and concentration of excess carriers.[15−17] Thus, U_{Dember} becomes 1−3 mV for the laser power range used. It can be shown that these values are overestimated, because eq 2 assumes that polarization takes part in one direction perpendicular to the surface, though in our system, the carriers diffuse along a semisphere, because of the nonuniform illumination geometry, which yields lower Δn and thus lower U_{Dember} in reality.

It is important to point out that for intrinsic and low-doping-level semiconductors, the sum $n_0 + bp_0$ in the denominator of the fraction in eq 2 is significantly lower compared to a heavily doped semiconductor, yielding a considerable change in the surface potential. In such cases, U_{Dember} can be as high as 30 mV with a positive pole in the illuminated area and a negative ring in the dark field, resulting in an annular-shaped deposition of metal film around the laser beam.[18]

Because of the temperature-dependent charge generation in semiconductors, an electric field $E_{\text{Seebeck}} = -\nabla U_{\text{Seebeck}} = \alpha \nabla T$ is established in the sample in which a temperature gradient ∇T is set up. The phenomenon is called the Seebeck effect, and the coefficient α, which ties the potential and temperature gradients together, is the so-called thermoelectric power (or Seebeck coefficient). The thermoelectric power depends on the temperature and on the slope S of the carrier mobility μ versus temperature, as well as on the concentration of holes p (or ionized acceptors), as [19]

$$\alpha = \frac{k}{e}\left(\frac{5}{2} + S + \ln\frac{N_{\text{v}}}{p}\right) \tag{3}$$

where $N_{\text{v}} = 2(2\pi m_p^* kT/h^2)^{3/2}$ is the density of states in the valence band (h is Planck's constant). Considering $\mu \propto T^{-2.2}$ (i.e., $S = -2.2$),[20] the calculated thermoelectric power is between 2.15 and 2.40 mV/K for the temperature range reached on the Si surface (Figure 3 inset). Thus, the Seebeck potential U_{Seebeck} formed between any points of the surface having difference in their temperature is obtained as

$$U_{\text{Seebeck}} = -\int_{T_1}^{T_2} \alpha \, dT \tag{4}$$

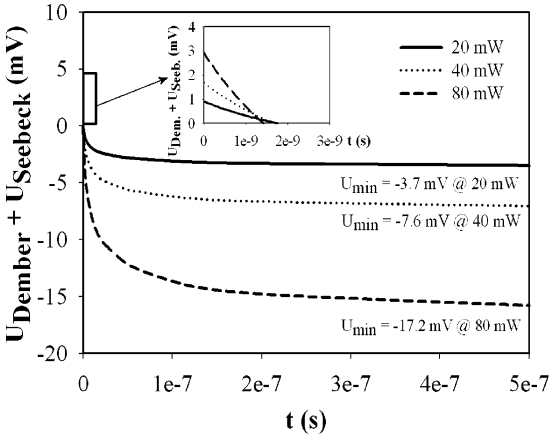

Figure 4. Temporal evolution of the sum of U_{Dember} and U_{Seebeck} on p$^+$-Si in the center of the laser spot having powers of 20, 40, and 80 mW. The inset shows how the positive surface potential (caused by the Dember effect) vanishes because of the increasing negative thermoelectromotive force (Seebeck effect).

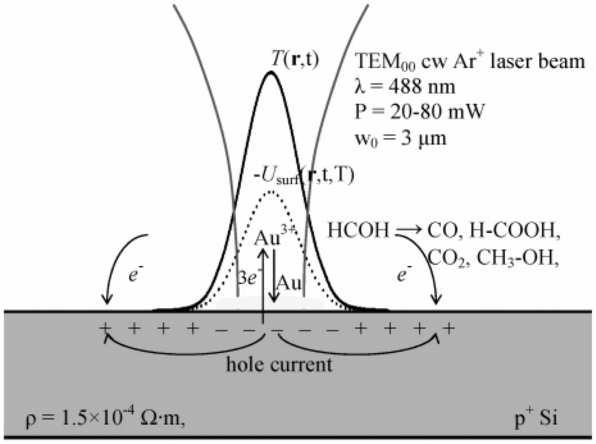

Figure 5. Schematic illustration of the supposed laser-assisted gold deposition mechanism on p$^+$-Si from the solution of NaAuCl$_4$ and HCOH. The minority carriers reduce gold ions, while a hole current flows from the illuminated volume, resulting in a positive surface in the dark zones, where formaldehyde is oxidized.

For the applied 20−80 mW laser powers, the maxima of U_{Seebeck} are between −3.6 and −17.2 mV (Figure 3).

Because the heated surface becomes negative, it acts as a cathode and enables the reduction of gold ions, $\text{Au}^{3+} + 3\text{e}^- \rightarrow \text{Au}$, while the dark areas undergo oxidation, $\text{Si} \rightarrow \text{Si}^{n+} + n\text{e}^-$. It is important to point out that, in equilibrium, the obtained Seebeck potential is not reduced by the Dember potential, because U_{Dember} suddenly decreases and then disappears as the first gold seeds are deposited, because the surface becomes shadowed from the laser beam disabling photogeneration of the electron−hole pair. The temporal evolution of the two potentials can be obtained simply by combining the calculated $T(t)$ functions with eqs 2 and 4.

As shown in Figure 4, the surface is positive at the beginning of the laser−Si interaction, because U_{Dember} forms right after the pair generation and diffusion. U_{Seebeck} arises together with the increasing temperature and needs ~2 ns to overcome U_{Dember} (in fact, U_{Dember} also increases, but the change is insignificant compared to U_{Seebeck}). As the surface becomes negative, the localized gold plating begins to cause negative feedback on the Dember effect, which in turn stops, where the process is governed by the Seebeck effect.

As observed in the course of our experiments, the film growth cannot proceed without additional formaldehyde in the precursor solution. This is because the electron transfer from the surface to the Au^{3+} ions is not compensated for, and so, the electric field and, consequently, the surface potential vanishes. When applying an electron source, which is HCOH in our case, the consumed electrons are compensated for and the localized plating process is maintained as long as the electron source is present (Figure 5). This surface-mediated reaction mechanism is also supported with the experiments carried out on wafers with and without thermal oxide on their surface. When the surface oxide is thin and not continuous (native oxide), the charge transport is enabled via tunneling and leaking. The electron transfer through a thick thermal surface oxide layer is disabled; therefore, the plating process is not possible.

Conclusions

Although laser-induced metal deposition on semiconductors from aqueous precursors has been investigated widely for more than ten years, there are several open questions still to be answered. In this paper, a new approach has been applied for describing both the spatial and temporal evolution of potentials. The finite-element method has been utilized to reveal surface temperature profiles under different laser power, and the results are used for calculating the arising Dember and Seebeck effects. The experimental observations are explained by means of a theory for charge transfer taking place between the polarized surface and the precursor. The theory supports both the dot- and ring-shaped metal deposition phenomena found previously on Si surfaces, considering the contribution of the positive Dember potential to the negative Seebeck voltage for various cases.

Acknowledgment. Géza Tóth would like to thank the EMPART Research Group of Infotech Oulu for financial support. Krisztián Kordás is grateful for the Academy Research Fellow post received from the Academy of Finland (Dnro 209414 and 213403) and also for the Nokia Visiting Scholarship given by the Nokia Foundation. This work was supported by the U.S. Army Research Development and Engineering Command Acquisition Center. The content of the information does not necessarily reflect the position or the policy of the federal government, and no official endorsement should be inferred.

References and Notes

(1) von Gutfield, R. J.; Tynan, E. E.; Meicher, R. L.; Blum, S. E. *Appl. Phys. Lett.* **1979**, *35*, 651.

(2) Micheels, R. H.; Darrow, A. D.; Rauh R. D. *Appl. Phys. Lett.* **1981**, *39*, 418.

(3) Karlicek, R. F.; Donnelly, V. M.; Collins, G. J. *J. Appl. Phys.* **1982**, *53*, 1084.

(4) Rose, T. L.; Longendorfer, D. H.; Rauh, R. D. *Appl. Phys. Lett.* **1983**, *42*, 193.

(5) Nánai, L.; Hevesi, I.; Bunkin, F. V.; Luklyanchuk, B. S.; Brook, M. R.; Shafeev, G. A.; Jelski, D. A.; Wu, Z. C.; George, T. F. *Appl. Phys. Lett.* **1989**, *54*, 736.

(6) Kautek, W.; Sorg, N.; Paatsch, W. *Electrochim. Acta* **1991**, *36*, 1803.

(7) Braga, A. K. de-M.; Baranauskas, V.; Peled, A. *Appl. Surf. Sci.* **1994**, *79*/*80*, 375.

(8) Diesinger, H.; Bsiesy, A.; Hérino, R. *J. Appl. Phys.* **2001**, *90*, 4862.

(9) Scheck, C.; Liu, Y.-K.; Evans, P.; Schad, R.; Bowers, A.; Zangari, G.; Williams, J. R.; Issacs-Smith, T. F. *Phys. Rev. B* **2004**, *69*, 35334.

(10) Kronik, L.; Sapira, Y. *Surf. Sci. Rep.* **1999**, *37*, 1.

(11) Schroder, D. K. *Meas. Sci. Technol.* **2001**, *12*, R16.

(12) Mizsei, J. *Vacuum* **2002**, *67*, 59−67.

(13) Chun, S. K. *J. Appl. Phys.* **1996**, *80*, 4773.

(14) Tzanetakis, P.; Kopidakis, N.; Fritzsche, H. *J. Non-Cryst. Solids* **1996**, *198*−*200*, 276.

(15) Hahneiser, O.; Kunst, M. *J. Appl. Phys.* **1999**, *85*, 7741.

(16) Cuevas, A.; Macdonald, D. *Sol. Energy* **2004**, *76*, 255−262.

(17) Kerra, M. J.; Cuevas, A. *J. Appl. Phys.* **2002**, *91*, 2473.

(18) Bäuerle, D. *Laser Processing and Chemistry*; Springer-Verlag: Berlin, 1996; pp 387−396.

(19) Kireev, P. S. *Semiconductor Physics*; Mir Publishers: Moscow, 1978; pp 318−334.

(20) Sze, S. M. *Physics of Semiconductor Devices*; Wiley: New York, 1981; pp 28−29.